

1 **Feasibility analysis of using inverse modeling for estimating field-scale evapotranspiration in**
2 **maize and soybean fields from soil water content monitoring networks**

3

4 Foad Foolad¹, Trenton E. Franz², Tiejun Wang^{2,3}, Justin Gibson², Ayse Kilic^{1,2}, Richard G. Allen⁴,
5 Andrew Suyker²

6

7 ¹Civil Engineering Department, University of Nebraska-Lincoln, USA

8 ²School of Natural Resources, University of Nebraska-Lincoln, USA

9 ³Institute of Surface-Earth System Science, Tianjin University, P.R. China

10 ⁴Kimberly Research and Extension Center, University of Idaho, USA

11

12 **Keywords:** Evapotranspiration; Soil Water Content; Inverse Modeling; Soil Hydraulic Parameters;
13 Cosmic-Ray Neutron Probe

14 Corresponding author T.E. Franz (tfranz2@unl.edu)

15

16

17

18

19 **Abstract**

20 In this study the feasibility of using inverse vadose zone modeling for estimating field scale actual
21 evapotranspiration (ET_a) was explored at a long-term agricultural monitoring site in eastern
22 Nebraska. Data from both point scale soil water content (SWC) sensors and the area-average
23 technique of Cosmic-Ray Neutron Probes were evaluated against independent ET_a estimates from a
24 co-located Eddy-Covariance tower. While this methodology has been successfully used for
25 estimates of groundwater recharge, it was essential to assess the performance of other components
26 of the water balance such as ET_a . In light of the recent evaluation of Land Surface Model (LSM)
27 performance from the plumber experiment, independent estimates of hydrologic state variables and
28 fluxes are critically needed benchmarks. The results here indicate reasonable estimates of daily and
29 annual ET_a from the point sensors, but with highly varied soil hydraulic function parameterizations
30 due to local soil texture variability. The results of multiple soil hydraulic parameterizations leading
31 to equally good ET_a estimates is consistent with the hydrological principle of equifinality. While this
32 study focused on one particular site, the framework can be easily applied to other SWC monitoring
33 networks across the globe. The value added products of groundwater recharge and ET_a flux from the
34 SWC monitoring networks will provide additional and more robust benchmarks for the validation of
35 LSM that continues to improve their forecast skill. In addition, the value added products of
36 groundwater recharge and ET_a often have more direct impacts on societal decision making than SWC
37 alone. Water flux impacts human decision making from policies on the long-term management of
38 groundwater resources (recharge), to yield forecasts (ET_a), and to optimal irrigation scheduling (ET_a).
39 Illustrating the societal benefits of SWC monitoring is critical to insure the continued operation and
40 expansion of these public datasets.

41

42 **1. Introduction**

43 Evapotranspiration (*ET*) is an important component in terrestrial water and surface energy
44 balance. In the United States, *ET* comprises about 75% of annual precipitation, while in arid and
45 semiarid regions *ET* comprises more than 90% of annual precipitation (Zhang et al., 2001; Glenn et
46 al., 2007; Wang et al., 2009a). As such, an accurate estimation of *ET* is critical in order to predict
47 changes in hydrological cycles and improve water resource management (Suyker et al., 2008;
48 Anayah and Kaluarachchi, 2014). Given the importance of *ET*, an array of measurement techniques
49 at different temporal and spatial scales have been developed (c.f., Maidment, 1992; Zhang et al.,
50 2014), including lysimeter, Bowen ratio, Eddy-Covariance (EC), and satellite-based surface energy
51 balance approaches. However, simple, low-cost, and accurate field-scale measurements of actual *ET*
52 (ET_a) still remain a challenge due to the uncertainties of available estimation techniques (Wolf et al.,
53 2008; Li et al., 2009; Senay et al., 2011; Stoy, 2012). For instance, field techniques, such as EC and
54 Bowen ratio, can provide relatively accurate estimation of local ET_a , but are often cost prohibitive
55 for wide-spread use beyond research applications (Baldocchi et al., 2001; Irmak, 2010). By
56 comparison, satellite-based remote sensing techniques are far less costly for widespread spatial
57 coverage (Allen et al., 2007), but are limited by their accuracy, temporal sampling frequency (e.g.,
58 Landsat 8 has a 16-day overpass), and technical issues that further limit temporal sampling periods
59 (e.g., cloud coverage during overpass) (Chemin and Alexandridis, 2001; Xie et al., 2008; Li et al.,
60 2009; Kjaersgaard et al., 2012).

61 As a complement to the above mentioned techniques, recent studies have used process-based
62 vadose zone models (VZMs) for estimating field-scale ET_a with reasonable success, particularly in
63 arid and semi-arid areas (Twarakavi et al., 2008; Izadifar and Elshorbagy, 2010; Galleguillos et al.,
64 2011; Wang et al., 2016). Although VZMs are time and cost effective for estimating field-scale ET_a ,

65 they generally require complex model parameterizations and inputs, some of which are not readily
66 available (e.g., soil hydraulic parameters and plant physiological parameters; c.f. Wang et al., 2016).
67 In order to address the issue of missing soil hydraulic parameters, a common approach is to use
68 pedotransfer functions to convert readily available soil information (e.g., texture, bulk density, etc.)
69 to soil hydraulic parameters (Wösten et al., 2001); however, significant uncertainties are usually
70 associated with this method for estimating local scale water fluxes (Wang et al., 2015). In fact,
71 Nearing et al. (2016) identified soil hydraulic property estimation as the largest source of information
72 lost when evaluating different land surface modeling schemes versus a soil moisture benchmark.
73 Poor and uncertain parameterization of soil hydraulic properties is a clear weakness of land surface
74 models (LSMs) predictive skill in sensible and latent heat fluxes (Best et al., 2015). This problem
75 will continue to compound with the continuing spatial refinement of hyper-resolution LSM grid cells
76 to less than 1 km (Wood et al., 2011).

77 In order to address the challenge of field scale estimation of soil hydraulic properties, here
78 we utilize inverse modeling for estimating soil hydraulic parameters based on field measurements
79 of soil water content (*SWC*) (c.f. Hopmans and Šimunek, 1999; Ritter et al., 2003). While VZM-
80 based inverse modeling approaches have already been examined for estimating groundwater
81 recharge (e.g., Jiménez-Martínez et al., 2009; Andreasen et al., 2013; Min et al., 2015; Ries et al.,
82 2015; Turkeltaub et al., 2015; Wang et al., 2016), its application for ET_a estimation has not been
83 adequately tested. Moreover, we note that simultaneous estimation of *SWC* states and surface energy
84 fluxes within LSMs is complicated by boundary conditions, model parameterization, and model
85 structure (Nearing et al., 2016). With the incorporation of regional soil datasets in LSMs like Polaris
86 (Chaney et al., 2016), effective strategies for estimating ground truth soil hydraulic properties from

87 existing *SWC* monitoring networks (e.g., SCAN, CRN, COSMOS, State/National Mesonets, c.f. Xia
88 et al. (2015)) will become critical for continuing to improve the predictive skill of LSMs.

89 The aim of this study is to examine the feasibility of using inverse VZM modeling for
90 estimating field scale ET_a based on long-term local meteorological and *SWC* observations for an
91 Ameriflux (Baldocchi et al., 2001) EC site in eastern Nebraska, USA. We note that while this study
92 focused on one particular study site in eastern Nebraska, the methodology can be easily adapted to
93 a variety of *SWC* monitoring networks across the globe (Xia et al., 2015), thus providing an extensive
94 set of benchmark data for use in LSMs. The remainder of the paper is organized as follows. In the
95 methods section we will describe the widely used VZM, Hydrus-1D (Šimunek et al., 2013), used to
96 obtain soil hydraulic parameters. We will assess the feasibility of using both profiles of in-situ *SWC*
97 probes as well as the area-average *SWC* technique from Cosmic-Ray Neutron Probes (CRNP). In
98 the results section we will compare simulated ET_a resulted from calibrated VZM with independent
99 ET_a estimates provided by EC observations. Finally a sensitivity analysis of key soil and plant
100 parameters will be presented.

101

102 **2. Materials and Methodology**

103 **2.1 Study Site**

104 The study site is located in eastern Nebraska, USA at the University of Nebraska Agricultural
105 and Development Center near Mead. The field site (US-Ne3, Figure 1a, 41.1797° N, 96.4397° W)
106 is part of the Ameriflux Network (Baldocchi et al., 2001) and has been operating continually since
107 2001. The regional climate is of a continental semiarid type with a mean annual precipitation of 784
108 mm/year (according to the Ameriflux US-Ne3 website). According to the Web Soil Survey Data

109 (Soil Survey Staff, 2016, <http://websoilsurvey.nrcs.usda.gov/>), the soils at the site are comprised
110 mostly of silt loam and silty clay loam (Figure 1b and Table 1). Soybean and maize are rotationally
111 grown at the site under rainfed conditions, with the growing season beginning in early May and
112 ending in October (Kalfas et al., 2011). Since 2001, crop management practices (i.e., planting density,
113 cultivars, irrigation, and herbicide and pesticide applications) have been applied in accordance with
114 standard best management practices prescribed for production-scale maize systems (Suyker et al.,
115 2008). More detailed information about site conditions can be found in Suyker et al. (2004) and
116 Verma et al. (2005).

117 An EC tower was constructed at the center of the field (Figure 1 and Figure 2a), which
118 continuously measures water, energy, and CO₂ fluxes (e.g., Baldocchi et al., 1988). At this field,
119 sensors are mounted at 3.0 m above the ground when the canopy is shorter than 1.0 m. At canopy
120 heights greater than 1.0 m, the sensors are then moved to a height of 6.2 m until harvest in order to
121 have sufficient upwind fetch (in all directions) representative of the cropping system being studied
122 (Suyker et al., 2004). In this study, hourly latent heat flux measurements were integrated to daily
123 values and then used for calculating daily EC ET_a integrated over the field scale. Detailed
124 information on the EC measurements and calculation procedures for ET_a are given in Suyker and
125 Verma (2009). Hourly air temperature, relative humidity, horizontal wind speed, net radiation, and
126 precipitation were also measured at the site. Destructive measurements of leaf area index (LAI) were
127 made every 10 to 14 days during the growing season at the study site (Suyker et al., 2005). We note
128 that the LAI data were linearly interpolated to provide daily estimates. Theta probes (TP) (Delta-T
129 Devices, Cambridge, UK) were installed at 4 locations in the study field with measurement depths
130 of 10, 25, 50, and 100 cm at each location to monitor hourly SWC in the root zone (Suyker et al.,
131 2008). Here, we denote these four locations as TP 1 (41.1775° N, 96.4442° W), TP 2 (41.1775° N,

132 96.4428° W), TP 3 (41.1775° N, 96.4402° W), and TP 4 (41.1821° N, 96.4419° W) (Figure 1b).
133 Daily precipitation (P) and reference evapotranspiration (ET_r) computed for the tall (alfalfa)
134 reference crop using the ASCE standardized Penman-Monteith equation (ASCE-EWRI 2005) are
135 shown in Figure 3 for the study period (2007–2012) at the study site.

136 In addition, a CRNP (model CRS 2000/B, HydroInnova LLC, Albuquerque, NM, USA,
137 41.1798 N°, 96.4412° W) was installed near the EC tower (Figure 1b and 2b) on 20 April 2011. The
138 CRNP measures hourly moderated neutron counts (Zreda et al., 2008, 2012), which are converted
139 into SWC following standard correction procedures and calibration methods (c.f., Zreda et al., 2012).
140 In addition, the changes in above-ground biomass were removed from the CRNP estimates of SWC
141 following Franz et al. (2015). The CRNP measurement depth (Franz et al., 2012) at the site varies
142 between 15-40 cm, depending on SWC . Note for simplicity in this analysis we assume the CRNP
143 has an effective depth of 20 cm (mean depth of 10 cm) for all observational periods. The areal
144 footprint of the CRNP is $\sim 250 \pm 50$ m radius circle (see Desilets and Zreda 2013 and Köhli et al.,
145 2015 for details). Here we assume for simplicity the EC and CRNP footprints are both representative
146 of the areal-average field conditions.

147

148 **2.2. Model setup**

149 **2.2.1 Vadose Zone Model**

150 The Hydrus-1D model (Šimunek et al., 2013), which is based on the Richards equation, was
151 used to calculate ET_a . The setup of the Hydrus-1D model is explained in detail by Jiménez-Martínez
152 et al. (2009), Min et al. (2015), and Wang et al. (2016), and only a brief description of the model
153 setup is provided here. Given the measurement depths of the Theta Probes, the simulated soil profile

154 length was chosen to be 175 cm with 176 nodes at 1 cm intervals. An atmospheric boundary
 155 condition with surface runoff was selected as the upper boundary. This allowed the occurrence of
 156 surface runoff when precipitation rates were higher than soil infiltration capacity or if the soil
 157 became saturated. According to a nearby USGS monitoring well (Saunders County, NE, USGS
 158 411005096281502, ~2.7 km away), the depth to water tables was greater than 12 m during the study
 159 period. Therefore, free drainage was used as the lower boundary condition.

160 Daily ET_r was calculated using the ASCE Penman-Monteith equation for the tall (0.5 m)
 161 ASCE reference (ASCE-EWRI, 2005), and daily potential evapotranspiration (ET_p) was calculated
 162 according to FAO 56 (Allen et al., 1998):

$$163 \quad ET_p(t) = K_C(t) \times ET_r(t) \quad (1)$$

164 where K_C is a crop-specific coefficient at time t . The estimates of growth stage lengths and K_C values
 165 for maize and soybean suggested by Allen et al. (1998) and Min et al. (2015) were adopted in this
 166 study. In order to partition daily ET_p into potential transpiration (T_p) and potential evaporation (E_p)
 167 as model inputs, Beer's law (Šimunek et al., 2013) was used as follows:

$$168 \quad E_p(t) = ET_p(t) \times e^{-k \times LAI(t)} \quad (2)$$

$$169 \quad T_p(t) = ET_p(t) - E_p(t) \quad (3)$$

170 where k [-] is an extinction coefficient with a value set to 0.5 (Wang et al., 2009b) and LAI [L^2/L^2]
 171 is leaf area index described in the previous section. The root water uptake, $S(h)$, was simulated
 172 according to the model of Feddes et al. (1978):

$$173 \quad S(h) = \alpha(h) \times S_p \quad (4)$$

174 where $\alpha(h)$ [-] is the root-water uptake water stress response function and varies between 0 and 1
 175 depending on soil matric potentials, and S_p is the potential water uptake rate and assumed to be equal
 176 to T_p . The summation of actual soil evaporation and actual transpiration is ET_a .

177 Since the study site has annual cultivation rotations between soybean and maize, the root growth
 178 model from the Hybrid-Maize Model (Yang et al., 2004) was used to model the root growth during
 179 the growing season:

$$180 \begin{cases} \text{if } D < MRD, D = \frac{AGDD}{GDD_{Silking}} MRD \\ \text{or } D = MRD \end{cases} \quad (5)$$

181 where D (cm) is plant root depth for each growing season day, MRD is the maximum root depth
 182 (assumed equal to 150 cm for maize and 120 cm for soybean in this study following Yang et al.,
 183 2004), $AGDD$ is the accumulated growing degree days, and $GDD_{Silking}$ is the accumulated GDD at
 184 the silking point (e.g., accumulated plant GDD approximately 60-70 days after crop emergence).
 185 GDD for each growing season day was calculated as:

$$186 GDD = \frac{T_{max} - T_{min}}{2} - T_{base} \quad (6)$$

187 where T_{max} and T_{min} are the maximum and minimum daily temperature ($^{\circ}\text{C}$), respectively, and T_{base}
 188 is the base temperature set to be 10°C following McMaster and Wilhelm (1997) and Yang et al.
 189 (1997). Finally, the Hoffman and van Genuchten (1983) model was used to calculate root
 190 distribution. Further details about the model can be found in Šimunek et al. (2013).

191

192 2.2.2 Inverse modeling to estimate soil hydraulic parameters

193 Inverse modeling was used to estimate soil hydraulic parameters for the van Genuchten-
 194 Mualem model (Mualem, 1976; van Genuchten, 1980):

$$195 \theta(h) = \begin{cases} \theta_r + \frac{\theta_s - \theta_r}{(1 + |\alpha h|^n)^m}, & h < 0 \\ \theta_s, & h \geq 0 \end{cases} \quad (7)$$

$$196 K(S_e) = K_s \times S_e^l \times [1 - (1 - S_e^{1/m})^m]^2 \quad (8)$$

197 where θ [L^3/L^3] is volumetric *SWC*; θ_r [L^3/L^3] and θ_s [L^3/L^3] are residual and saturated moisture
 198 content, respectively; h [L] is pressure head; K [L/T] and K_s [L/T] are unsaturated and saturated
 199 hydraulic conductivity, respectively; and $S_e (= (\theta - \theta_r) / (\theta_s - \theta_r))$ [-] is saturation degree. With respect to
 200 the fitting factors, α [1/L] is inversely related to air entry pressure, n [-] measures the pore size
 201 distribution of a soil with $m = 1 - 1/n$, and l [-] is a parameter accounting for pore space tortuosity and
 202 connectivity.

203 Daily *SWC* data from the four TP locations and CRNP location were used for the inverse
 204 modeling. Based on the measurement depths of the TPs, the simulated soil columns were divided
 205 into four layers for TP locations (i.e., 0-15 cm, 15-35 cm, 35-75 cm, and 75-175 cm), which led to
 206 a total of 24 hydraulic parameters (θ_r , θ_s , α , n , K_s , and l) to be optimized based on observed *SWC*
 207 values. In order to efficiently optimize the parameters, we used the method outlined in Turkeltaub
 208 et al. (2015). Since Hydrus-1D is limited to optimizing a maximum of 15 parameters at once and
 209 that the *SWC* of the lower layers changes more slowly and over a smaller range than the upper layers,
 210 the van Genuchten parameters of the upper two layers were first optimized, while the parameters of
 211 the lower two layers were fixed. Then, the optimized van Genuchten parameters of the upper two
 212 layers were kept constant, while the parameters of the lower two layers were optimized. The process
 213 was continued until there were no further improvements in the optimized hydraulic parameters or
 214 until the changes in the lowest sum of squares were less than 0.1%. Given the sensitivity of the

215 optimization results to the initial guesses of soil hydraulic parameters in the Hydrus model, soil
216 hydraulic parameters from six soil textures were used as initial inputs for the optimizations at each
217 location (Carsel and Parish, 1988), including sandy clay loam, silty clay loam, loam, silt loam, silt,
218 and clay loam. Based on the length of available *SWC* data from the TP measurements, the periods
219 of 2007, 2008-2010, and 2011-2012 were used as the spin-up, calibration, and validation periods,
220 respectively. Moreover, to minimize the impacts of freezing conditions on the quality of *SWC*
221 measurements, data from January to March of each calendar year were removed (based on available
222 soil temperature data) from the optimizations.

223 In addition to the TP profile observations, we used the CRNP area-average *SWC* in the
224 inverse procedure to develop an independent set of soil parameters. The CRNP was assumed to
225 provide *SWC* data with an average effective measurement depth of 20 cm at this study site. The
226 observation point was therefore set at 10 cm. As a first guess and in the absence of other information,
227 soil properties were assumed to be homogeneous throughout the simulated soil column with a length
228 of 175 cm. Because the CRNP was installed in 2011 at the study site, the periods of 2011, 2012-
229 2013, and 2014 were used as spin-up, calibration, and validation periods, respectively, for the
230 optimization procedure.

231 The lower and upper bounds of each van Genuchten parameter are provided in Table 2. With
232 respect to the goodness-of-fit assessment, Root Mean Square Error (RMSE) between simulated and
233 observed *SWC* was chosen as the objective function to minimize in order to estimate the soil
234 hydraulic parameters. The built in optimization procedure in Hydrus-1D was used to perform
235 parameter estimation. A sensitivity analysis of the six soil model parameters was performed. In
236 addition, three additional performance criteria, including Coefficient of Determination (R^2), Mean

237 Average Error (MAE), and the Nash-Sutcliffe Efficiency (NSE) were used to further evaluate and
 238 validate the selected model behavior:

$$239 \quad RMSE = \sqrt{\frac{1}{n} \sum_{i=1}^n (P_i - O_i)^2} \quad (9)$$

$$240 \quad R^2 = \left(\frac{n(\sum_{i=1}^n P_i O_i) - (\sum_{i=1}^n P_i)(\sum_{i=1}^n O_i)}{\sqrt{[n \sum_{i=1}^n P_i^2 - (\sum_{i=1}^n P_i)^2][n \sum_{i=1}^n O_i^2 - (\sum_{i=1}^n O_i)^2]}} \right)^2 \quad (10)$$

$$241 \quad MAE = \frac{1}{n} \sum_{i=1}^n |P_i - O_i| \quad (11)$$

$$242 \quad NSE = 1 - \frac{\sum_{i=1}^n (P_i - O_i)^2}{\sum_{i=1}^n (O_i - \bar{O}_i)^2} \quad (12)$$

243 where n is the total number of *SWC* data points, O_i , and P_i , are respectively the observed and
 244 simulated daily *SWC* on day i , and \bar{O}_i is the observed mean value. Based on the best scores (i.e.,
 245 lowest RMSE values), the best optimized set of soil hydraulic parameters at each location were
 246 selected. Using the selected parameters, the Hydrus model was then run in a forward mode in order
 247 to estimate ET_a between 2007 and 2012. Finally, we note that the years 2004-2006 were used as a
 248 model spin-up period for the forward model and evaluation of ET_a because of the longer climate
 249 record length.

250

251 **3. Results and Discussions**

252 **3.1 Vadose Zone Inverse Modeling Results**

253 The time series of the average *SWC* from the four TP locations along with one standard
 254 deviation at each depth are plotted in Figure 4. Based on the large standard deviation values (Figure
 255 4), despite the relatively small spatial scale (~65 ha) and uniform cropping at the study site, *SWC*

256 varies considerably across the site, particularly during the growing season. The comparison between
257 *SWC* data from the CRNP and spatial average of *SWC* data at the four TP locations in the study field
258 (i.e. average of 10 and 25 cm depths at TP locations) is presented in Figure 5. The daily RMSE
259 between the spatial average of the TPs and CRNP data is $0.037 \text{ cm}^3/\text{cm}^3$, which is consistent with
260 other studies that reported similar values in semiarid shrublands (Franz et al., 2012), German Forests
261 (Bogena et al., 2013, Baatz et al., 2014), montane forests in Utah (Lv et al., 2014), sites across
262 Australia (Hawdon et al., 2014), and a mixed land use agricultural site in Austria (Franz et al. 2016).
263 We note that we would expect lower RMSE ($\sim < 0.02 \text{ cm}^3/\text{cm}^3$) with additional point sensors located
264 at shallower depths and in more locations distributed across the study site. Nevertheless, the
265 consistent behavior between the spatial mean *SWC* of TPs and the CRNP allows us to explore spatial
266 variability of soil hydraulic properties within footprint using inverse modeling. This will be
267 described in the next sections. The study period (2007-2012, Figure 6) contained significant inter-
268 annual variability in precipitation. During the spin-up period in 2007, the annual precipitation (942
269 mm) was higher than the mean annual precipitation (784 mm), 2008 was a wet year (997 mm), 2009-
270 2011 were near average years (715 mm), and 2012 was a record dry year (427 mm) with widespread
271 drought across the region. Therefore, both wet and dry years were considered in the inverse modeling
272 simulation period.

273 As an illustration, Figure 7 shows the daily observed and simulated *SWC* during the
274 calibration (2008–2010) and validation (2011–2012) periods at the TP 1 location (the simulation
275 results of the other three sites can be found in the supplemental Figures S1, S2, and S3). The results
276 of objective function criterion (RMSE) and the other three performance criteria (e.g., R^2 , MAE, and
277 NSE) between simulated and observed *SWC* values at TPs locations are presented in Table 3.

278 In this research we define RMSE values less than $0.03 \text{ cm}^3/\text{cm}^3$ between observed and
279 simulated *SWC* values as well-matched and RMSE between 0.03 and $0.06 \text{ cm}^3/\text{cm}^3$ as fairly well-
280 matched. We note the target error range of satellite *SWC* products (e.g. SMOS and SMAP) is less
281 than $0.04 \text{ cm}^3/\text{cm}^3$ (Entekhabi et al., 2010). Similar to previous studies (e.g., Jiménez-Martínez et
282 al., 2009; Andreasen et al., 2013; Min et al., 2015; Wang et al., 2016), the results of all the
283 performance criteria at TP locations show the capability of inverse modeling in estimation of soil
284 hydraulic parameters. The results of the calibration period (2008-2010) indicate that the simulated
285 and observed *SWC* values are in good agreement (i.e. well matched as defined above) throughout
286 the entire period at most locations and depths (Figure 7 and Table 3). In addition, the simulated and
287 observed *SWC* data are fairly well-matched at most locations and depths during the validation period
288 (2011-2012), with notable differences during the second half of 2012 during the extreme drought
289 conditions (Figure 7 and Table 3). Reasons for this disagreement in the observed and simulated *SWC*
290 data will be discussed in the following sections.

291 The results of inverse modeling using the CRNP data also indicate the feasibility of using
292 these data to estimate effective soil hydraulic parameters (Figure 8 and Table 4). Based on the
293 performance criteria (Table 4), the simulated data are fairly well-matched with the observed *SWC*
294 data during both the calibration and validation periods. Additional information from deeper soil
295 probes or more complex modeling approaches such as data assimilation techniques (Rosolem et al.,
296 2014, Renzullo et al., 2014) may be needed to fully utilize the CRNP data for the entire growing
297 season. However, this was beyond the scope of the current study and merits further investigation
298 given the global network of CRNP (Zreda et al., 2012) dating back to ~2011.

299 Table 5 summarizes the optimized van Genuchten parameters for the four different depths
300 of the four TP locations and the single layer for the CRNP location. The optimized parameters were

301 then used to estimate ET_a for the entire study period as an independent comparison to the EC ET_a
302 data. The results of the ET_a evaluation will be discussed in the next section. According to the
303 simulation results (Table 5), in most of the soil layers, the TP 4 location results in lower n , K_s , and
304 higher θ_r values than the other 3 locations (TPs 1-3), suggesting either underlying soil texture
305 variability in the field or texture dependent sensor sensitivity/calibration. As a validation for the
306 simulation results, the publicly available Web Soil Survey Data (<http://websoilsurvey.nrcs.usda.gov/>)
307 was used to explore whether the optimized van Genuchten parameters from the inverse modeling
308 (Figure 1b and Table 2) agreed qualitatively with the survey data. Based on the Web Soil Survey
309 Data, the soil at the TP 4 location contains higher clay percentage than the other locations.
310 Meanwhile, the optimized parameters reflect the spatial pattern of soil texture in the field as shown
311 by the Web Soil Survey Data (e.g., lower n and K_s values and higher θ_r values at the TP 4 location
312 with finer soil texture). Physically, finer-textured soils generally have lower K_s and higher θ_r values
313 (Carsel and Parrish, 1988). Moreover, the shape factor n is indicative of pore size distributions of
314 soils. In general, finer soils with smaller pore sizes tend to have lower n values (Carsel and Parrish,
315 1988). The observed SWC at the TP 4 location is consistently higher than the average SWC of the
316 other three locations (Figure S4 in supplemental materials), which can be partly attributed to the
317 higher θ_r values at the TP 4 location (Wang and Franz, 2015). Overall, the obtained van Genuchten
318 parameters from the inverse modeling are in qualitatively good agreement with the available spatial
319 distribution of soil texture in the study field, indicating the capability of using inverse VZM to infer
320 soil hydraulic properties. Further work on validating the Web Soil Survey Data soil hydraulic
321 property estimates is of general interest to the LSM community.

322

323 **3.2 Comparison of modeled ET_a with observed ET_a**

324 Because a longer set of climatic data was available at the study site (as compared to *SWC*
325 data), we used 2004-2006 as a spin-up period. Using the best fit soil hydraulic parameters for the
326 four TP locations and the single CRNP location, the Hydrus-1D model was then run in a forward
327 mode to calculate ET_a over the entire study period (2007-2012). The simulated daily ET_a was then
328 compared with the independent EC ET_a measurements using RMSE (Eq. (9)) as the evaluation
329 criterion. In order to upscale TP ET_a estimation to the field/EC scale, we used the soil textural
330 boundaries and areas defined by the Web Soil Survey Data map to compute a weighted average ET_a .
331 In this research we consider RMSE values less than 1 mm/day between observed and simulated ET_a
332 values as well-matched and RMSE values between 1 and 1.2 as fairly well-matched (Figure 9 and
333 Table 6). The performance criterion results indicate that the simulated daily ET_a is in a better
334 agreement with EC ET_a measurements at the TP 1-3 locations than at the TP 4 and CRNP locations
335 (Table 6). However, based on the performance criteria from inverse modeling results and on the
336 Web Soil Survey Data, we conclude that spatial heterogeneity of soil texture in the study field results
337 in significant spatial variation in ET_a rates across the field (e.g., less ET_a occurs at the TP 4 location
338 than from the other parts of the field). Here smaller ET_a rates at the TP 4 location are likely due to
339 finer soil texture at this location, which makes it more difficult for the plant/roots to overcome
340 potentials to extract water from the soil, thus leading to a lower ET_a rate and greater plant stress. In
341 addition, higher surface runoff can be expected at the TP 4 location due to finer-textured soils (as
342 we observed during our field campaigns). According to the simulation results the average surface
343 runoff at the TP 4 location was about 44.8 mm/year from 2007 to 2012, while the average surface
344 runoff at the other three locations (TPs 1-3) was around 10.6 mm/year, which partially accounts for
345 the lower ET_a rates. We note that future work using historic yield maps may also be used to further

346 elucidate the soil hydraulic property differences given the direct correlation between transpiration
347 and yield.

348 Given that CRNPs have a limited observational depth and that only one single soil layer was
349 optimized in the inverse model for the CRNP, one could expect the simulated daily ET_a from the
350 CRNP to have larger uncertainty. Here we found an RMSE of 1.14 mm/day using the CRNP versus
351 0.91 mm/day for the upscaled TP locations. However, when the optimized soil parameters obtained
352 from the CRNP data were used to estimate ET_a , the model did simulate daily ET_a fairly well during
353 both non-growing and growing seasons in comparison to the EC ET_a measurements.

354 On the annual scale, ET_a measured by the EC tower accounted for 87% of annual P recorded
355 at the site during the study period (Figure 6). Overall, the simulated annual ET_a at all the TP and
356 CRNP locations is comparable to the annual ET_a measured by the EC tower, except during 2012
357 (Table 7), in which a severe drought occurred in the region. One explanation is that the plants extract
358 more water from deeper layers under extreme drought conditions than what we defined as a
359 maximum rooting depth (150 cm for maize and 120 cm for soybean) for the model, thus limiting the
360 VZM ability to estimate ET_a accurately during the drought year (2012). In fact, based on the EC ET_a
361 measurements at the study site, there was just 8.18% reduction in annual ET_a in 2012 than the
362 average of the other years (2007-2011), while there were 29.58% and 35.75% reduction in annual
363 simulated ET_a values respectively in upscaled TP and CRNP. This shows that although 2012 was a
364 very dry year, the plants probably found most of the needed water by extracting water from deeper
365 soil reservoirs. As previously mentioned we defined a maximum rooting depth for the model that
366 could greatly impact the results. To further illustrate this point, a sensitivity analysis was performed
367 on the maximum rooting depth and presented in the following section. However, we note that given
368 the fact that EC ET_a estimation can have up to 20% uncertainty (Massman and Lee, 2002, and

369 Hollineger and Richardson, 2005), and accounting for the natural spatial variability of ET_a due to
370 soil texture and root depth growth uncertainties, the various ET_a estimation techniques performed
371 fairly well. In fact, it is difficult to identify which ET_a estimation method is the most accurate method.
372 These results are consistent with the concept of equifinality in hydrologic modeling given the
373 complexity of natural systems (Beven and Freer, 2001). Moreover, the findings here are consistent
374 with Nearing et al. (2016) that show information lost in model parameters greatly affects the soil
375 moisture comparisons against a benchmark. However, soil parameterization was less important in
376 the loss of information for the comparisons of ET /latent energy against a benchmark. Fully resolving
377 these issues remains a key challenge to the land surface modeling community and the model's ability
378 to make accurate predictions (Best 2015). The following section provides a detailed sensitivity
379 analysis of the soil hydraulic parameters and root depth growth functions in order to begin to
380 understand the sources of error in estimating ET_a from SWC monitoring networks.

381

382 **3.3 Sensitivity analysis of soil hydraulic parameters and rooting depth**

383 In this research we compared simulated ET_a with the measured EC ET_a . As expected some
384 discrepancies between simulated and measured ET_a values existed. In order to begin to understand
385 the key sources of error we performed a set of sensitivity analysis experiments on the estimated soil
386 hydraulic parameters. Building on Wang et al. (2009b), a sensitivity analysis for a single
387 homogeneous soil layer (6 parameters) and a 4-layer soil profile (24 parameters) was performed over
388 the study period (2007–2012). Here we performed a preliminary sensitivity analysis by changing a
389 single soil hydraulic parameter one at a time while keeping the other parameters constant (i.e. at the
390 average value). Figure 10 illustrates the sensitivity results on simulated ET_a , indicating the soil
391 hydraulic parameters have a range of sensitivities with tortuosity (l) being the least. We found that

392 n and α were the most sensitive, particularly in the shallowest soil layer. This sensitivity to the
393 shallowest soil layer provides an opportunity to use the CRNP observations, particularly in the early
394 growing season (i.e. when evaporation dominates latent energy flux), to help constrain estimates of
395 n and α . As the crop continues to develop (and transpiration contributes a relatively larger
396 component of latent energy) additional information about deeper soil layers should be used to
397 estimate soil hydraulic parameters or perform data assimilation. Moreover, the CRNP may be useful
398 in helping constrain and parameterize soil hydraulic functions in simpler evaporation models widely
399 used in remote sensing (c.f. Allen et al. 2007) and crop modeling (c.f. Allen et al. 1998).

400 Following the sensitivity analysis, we repeated the optimization experiment using only α , n ,
401 K_s , and used model default estimates for the other parameters in each layer. We found that the RMSE
402 values were significantly higher (1.511 vs. 0.911 mm/day) than when considering all 24 parameters.
403 We suspect that given the high correlation between soil hydraulic parameters (Carsel and Parrish
404 1988), that fixing certain parameters leads to a degradation in overall performance. We suggest
405 further sensitivity analyses, in particular changing multiple parameters simultaneously or using
406 multiple objective functions, be used to fully understand model behavior (c.f. Bastidas et al. 1999
407 and Rosolem et al. 2012).

408 A sensitivity analysis of ET_a by varying rooting depth is summarized in Figure 11. As would
409 be expected with increasing rooting depth, higher ET_a occurred. In addition, Figure 11 illustrates a
410 decreasing RMSE against EC observations for up to 200% increases. Again it is unclear if the EC
411 observations are biased high or in fact rooting depths are much greater than typically considered in
412 these models. The high observed EC values in the drought year of 2012 indicate that roots likely
413 uptake water from below the 1 m observations. Certainly the results shown here further indicate the
414 importance of root water uptake parameters in VZMs and LSMs, even in homogeneous annual

415 cropping systems. While beyond the scope of this paper we refer the reader to the growing literature
416 on the importance of root water uptake parameters on hydrologic fluxes (c.f. Schymanski et al. 2008
417 and Guswa 2012).

418

419 **4. Conclusions**

420 In this study the feasibility of using inverse vadose zone modeling for field scale ET_a
421 estimation was explored at an agricultural site in eastern Nebraska. Both point SWC sensors (TP)
422 and area-average techniques (CRNP) were explored. This methodology has been successfully used
423 for estimates of groundwater recharge but it was critical to assess the performance of other
424 components of the water balance such as ET_a . The results indicate reasonable estimates of daily and
425 annual ET_a but with varied soil hydraulic function parameterizations. The varied soil hydraulic
426 parameters were expected given the heterogeneity of soil texture at the site and consistent with the
427 principle of equifinality in hydrologic systems. We note that while this study focused on one
428 particular site, the framework can be easily applied to other networks of SWC monitoring across the
429 globe (Xia et al., 2015). The value added products of groundwater recharge and ET_a flux from the
430 SWC monitoring networks will provide additional and more robust benchmarks for the validation of
431 LSM that continue to improve their forecast skill.

432

433 **5. Data availability**

434 The climatic and EC data used in this research can be found at <http://ameriflux.lbl.gov/>. The
435 TP SWC and LAI data in the study site are provided by Dr. Andrew Suyker and CRNP SWC are

436 provided by Dr. Trenton E. Franz and both sets of data can be requested directly from the authors.
437 The US soil taxonomy information is provided by Soil Survey Staff and is available online at
438 <http://websoilsurvey.nrcs.usda.gov/> (accessed in July, 2016). The remaining datasets are provided
439 in the supplemental material associated with this paper.

440

441 **Acknowledgments**

442 This research is supported financially by the Daugherty Water for Food Global Institute at
443 the University of Nebraska, NSF EPSCoR FIRST Award, the Cold Regions Research Engineering
444 Laboratory through the Great Plains CESU, and an USGS104b grant. We sincerely appreciate the
445 support and the use of facilities and equipment provided by the Center for Advanced Land
446 Management Information Technologies, School of Natural Resources and data from Carbon
447 Sequestration Program, the University of Nebraska-Lincoln. TEF would like to thank Eric Wood for
448 his inspiring research and teaching career. No doubt the skills TEF learned while at Princeton in
449 formal course work, seminars, and discussions with Eric will serve him well in his own career.

450 **References**

- 451 Allen, R. G., Pereira, L. S., Raes, D., & Smith, M. (1998). Crop evapotranspiration-guidelines for
452 computing crop water requirements-FAO irrigation and drainage paper 56. FAO, Rome,
453 300(9), D05109.
- 454 Allen, R. G., Tasumi, M., & Trezza, R. (2007). Satellite-based energy balance for mapping
455 evapotranspiration with internalized calibration (METRIC)—Model. *Journal of Irrigation and*
456 *Drainage Engineering*, 133(4), 380-394.
- 457 Anayah, F. M., & Kaluarachchi, J. J. (2014). Improving the complementary methods to estimate
458 evapotranspiration under diverse climatic and physical conditions. *Hydrology and Earth*
459 *System Sciences*, 18(6), 2049-2064.
- 460 Andreasen, M., Andreasen, L. A., Jensen, K. H., Sonnenborg, T. O., & Bircher, S. (2013).
461 Estimation of regional groundwater recharge using data from a distributed soil moisture
462 network. *Vadose Zone Journal*, 12(3)
- 463 ASCE – EWRI. (2005). The ASCE Standardized reference evapotranspiration equation. ASCE-
464 EWRI Standardization of Reference Evapotranspiration Task Comm. Report, ASCE
465 Bookstore, ISBN 078440805, Stock Number 40805, 216 pages.
- 466 Baatz, R., Bogaen, H., Franssen, H. H., Huisman, J., Qu, W., Montzka, C., et al. (2014).
467 Calibration of a catchment scale cosmic-ray probe network: A comparison of three
468 parameterization methods. *Journal of Hydrology*, 516, 231-244.
- 469 Baldocchi, D. D., Hincks, B. B., & Meyers, T. P. (1988). Measuring biosphere-atmosphere
470 exchanges of biologically related gases with micrometeorological methods. *Ecology*, 1331-
471 1340.
- 472 Baldocchi, D., Falge, E., Gu, L., & Olson, R. (2001). FLUXNET: A new tool to study the temporal
473 and spatial variability of ecosystem-scale carbon dioxide, water vapor, and energy flux
474 densities. *Bulletin of the American Meteorological Society*, 82(11), 2415.

475 Bastidas, L. A., H. V. Gupta, S. Sorooshian, W. J. Shuttleworth, and Z. L. Yang (1999), Sensitivity
476 analysis of a land surface scheme using multicriteria methods, *J. Geophys. Res.-Atmos.*,
477 104(D16), 19481-19490. doi:10.1029/1999jd900155.

478 Best, M., Abramowitz, G., Johnson, H., Pitman, A., Balsamo, G., Boone, A., et al. (2015). The
479 plumbing of land surface models: Benchmarking model performance. *Journal of*
480 *Hydrometeorology*, 16(3), 1425-1442.

481 Beven, K., & Freer, J. (2001). Equifinality, data assimilation, and uncertainty estimation in
482 mechanistic modelling of complex environmental systems using the GLUE methodology.
483 *Journal of Hydrology*, 249(1), 11-29.

484 Bogena, H., Huisman, J., Baatz, R., Hendricks Franssen, H., & Vereecken, H. (2013). Accuracy of
485 the cosmic-ray soil water content probe in humid forest ecosystems: The worst case scenario.
486 *Water Resources Research*, 49(9), 5778-5791.

487 Carsel, R. F., & Parrish, R. S. (1988). Developing joint probability distributions of soil water
488 retention characteristics. *Water Resources Research*, 24(5), 755-769.

489 Chaney, N. W., Wood, E. F., McBratney, A. B., Hempel, J. W., Nauman, T. W., Brungard, C. W.,
490 et al. (2016). POLARIS: A 30-meter probabilistic soil series map of the contiguous United
491 States. *Geoderma*, 274, 54-67.

492 Chemin, Y., & Alexandridis, T. (2001). Improving spatial resolution of ET seasonal for irrigated
493 rice in Zhanghe, china. Paper Presented at the 22nd Asian Conference on Remote Sensing, 5.
494 pp. 9.

495 Desilets, D., & Zreda, M. (2013). Footprint diameter for a cosmic-ray soil moisture probe: Theory
496 and monte carlo simulations. *Water Resources Research*, 49(6), 3566-3575.

497 Entekhabi, D., E. G. Njoku, P. E. O'Neill, K. H. Kellogg, W. T. Crow, W. N. Edelstein, J. K.
498 Entin, S. D. Goodman, T. J. Jackson, J. Johnson, J. Kimball, J. R. Piepmeier, R. D. Koster, N.
499 Martin, K. C. McDonald, M. Moghaddam, S. Moran, R. Reichle, J. C. Shi, M. W. Spencer, S.

500 W. Thurman, L. Tsang, and J. Van Zyl (2010), The Soil Moisture Active Passive (SMAP)
501 Mission, Proc. IEEE, 98(5), 704-716. doi:10.1109/jproc.2010.2043918.

502 Feddes, R. A., Kowalik, P. J., & Zaradny, H. (1978). Simulation of field water use and crop yield.
503 Centre for Agricultural Publishing and Documentation.

504 Franz, T. E., Wahbi, A., Vreugdenhil, M., Weltin, G., Heng, L., Oismueller, M., et al. (2016).
505 Using cosmic-ray neutron probes to monitor landscape scale soil water content in mixed land
506 use agricultural systems. Applied and Environmental Soil Science, 2016.

507 Franz, T. E., Wang, T., Avery, W., Finkenbiner, C., & Brocca, L. (2015). Combined analysis of
508 soil moisture measurements from roving and fixed cosmic ray neutron probes for multiscale
509 real-time monitoring. Geophysical Research Letters, 42(9), 3389-3396.

510 Franz, T. E., Zreda, M., Ferre, T., Rosolem, R., Zweck, C., Stillman, S., et al. (2012).
511 Measurement depth of the cosmic ray soil moisture probe affected by hydrogen from various
512 sources. Water Resources Research, 48(8).

513 Galleguillos, M., Jacob, F., Prévot, L., Lagacherie, P., & Liang, S. (2011). Mapping daily
514 evapotranspiration over a Mediterranean vineyard watershed. Geoscience and Remote
515 Sensing Letters, IEEE, 8(1), 168-172.

516 Glenn, E. P., Huete, A. R., Nagler, P. L., Hirschboeck, K. K., & Brown, P. (2007). Integrating
517 remote sensing and ground methods to estimate evapotranspiration. Critical Reviews in Plant
518 Sciences, 26(3), 139-168.

519 Guswa, A. J. (2012), Canopy vs. Roots: Production and Destruction of Variability in Soil Moisture
520 and Hydrologic Fluxes, Vadose Zone Journal, 11(3). doi:10.2136/vzj2011.0159.

521 Hawdon, A., McJannet, D., & Wallace, J. (2014). Calibration and correction procedures for
522 cosmic-ray neutron soil moisture probes located across Australia. Water Resources Research,
523 50(6), 5029-5043.

- 524 Hollinger, D. Y., & Richardson, A. D. (2005). Uncertainty in eddy covariance measurements and
525 its application to physiological models. *Tree Physiology*, 25(7), 873-885.
- 526 Hopmans, J.W., Šimunek, J., 1999. Review of inverse estimation of soil hydraulic properties. In:
527 van Genuchten, M.Th. Leij, F.J., Wu, L. (Eds.), *Proceedings of the International Workshop*
528 *Characterization and Measurement of Hydraulic Properties of Unsaturated Porous Media*.
529 University of California, Riverside, 643–659. Irmak, S. (2010). Nebraska water and energy
530 flux measurement, modeling, and research network (NEBFLUX). *Transactions of the*
531 *ASABE*, 53(4), 1097-1115. Irmak, S. (2010). Nebraska water and energy flux measurement,
532 modeling, and research network (NEBFLUX). *Transactions of the ASABE*, 53(4), 1097-1115.
- 533 Izadifar, Z., & Elshorbagy, A. (2010). Prediction of hourly actual evapotranspiration using neural
534 networks, genetic programming, and statistical models. *Hydrological Processes*, 24(23), 3413-
535 3425.
- 536 Jiménez-Martínez, J., Skaggs, T., Van Genuchten, M. T., & Candela, L. (2009). A root zone
537 modelling approach to estimating groundwater recharge from irrigated areas. *Journal of*
538 *Hydrology*, 367(1), 138-149.
- 539 Kalfas, J. L., Xiao, X., Vanegas, D. X., Verma, S. B., & Suyker, A. E. (2011). Modeling gross
540 primary production of irrigated and rain-fed maize using MODIS imagery and CO₂ flux
541 tower data. *Agricultural and Forest Meteorology*, 151(12), 1514-1528.
- 542 Kjaersgaard, J., Allen, R., Trezza, R., Robinson, C., Oliveira, A., Dhungel, R., et al. (2012). Filling
543 satellite image cloud gaps to create complete images of evapotranspiration. *IAHS-AISH*
544 *Publication*, 102-105.
- 545 Köhli, M., Schrön, M., Zreda, M., Schmidt, U., Dietrich, P., & Zacharias, S. (2015). Footprint
546 characteristics revised for field-scale soil moisture monitoring with cosmic-ray neutrons.
547 *Water Resources Research*, 51(7), 5772-5790.

548 Li, Z., Tang, R., Wan, Z., Bi, Y., Zhou, C., Tang, B., et al. (2009). A review of current
549 methodologies for regional evapotranspiration estimation from remotely sensed data. *Sensors*,
550 9(5), 3801-3853.

551 Lv, L., Franz, T. E., Robinson, D. A., & Jones, S. B. (2014). Measured and modeled soil moisture
552 compared with cosmic-ray neutron probe estimates in a mixed forest. *Vadose Zone Journal*,
553 13(12)

554 Maidment, D. R. (1992). *Handbook of hydrology*. McGraw-Hill Inc.

555 Massman, W., & Lee, X. (2002). Eddy covariance flux corrections and uncertainties in long-term
556 studies of carbon and energy exchanges. *Agricultural and Forest Meteorology*, 113(1), 121-
557 144.

558 McMaster, G. S., & Wilhelm, W. (1997). Growing degree-days: One equation, two interpretations.
559 *Agricultural and Forest Meteorology*, 87(4), 291-300.

560 Min, L., Shen, Y., & Pei, H. (2015). Estimating groundwater recharge using deep vadose zone data
561 under typical irrigated cropland in the piedmont region of the north china plain. *Journal of*
562 *Hydrology*, 527, 305-315.

563 Mualem, Y. (1976). A new model for predicting the hydraulic conductivity of unsaturated porous
564 media. *Water Resources Research*, 12(3), 513-522.

565 Nearing, G. S., Mocko, D. M., Peters-Lidard, C. D., Kumar, S. V., & Xia, Y. (2016).
566 Benchmarking NLDAS-2 soil moisture and evapotranspiration to separate uncertainty
567 contributions. *Journal of Hydrometeorology*, 17(3), 745-759.

568 Renzullo, L. J., Van Dijk, A., Perraud, J., Collins, D., Henderson, B., Jin, H., et al. (2014).
569 Continental satellite soil moisture data assimilation improves root-zone moisture analysis for
570 water resources assessment. *Journal of Hydrology*, 519, 2747-2762.

571 Ries, F., Lange, J., Schmidt, S., Puhlmann, H., & Sauter, M. (2015). Recharge estimation and soil
572 moisture dynamics in a Mediterranean, semi-arid karst region. *Hydrology and Earth System*
573 *Sciences*, 19(3), 1439-1456.

574 Ritter, A., Hupet, F., Muñoz-Carpena, R., Lambot, S., & Vanclooster, M. (2003). Using inverse
575 methods for estimating soil hydraulic properties from field data as an alternative to direct
576 methods. *Agricultural Water Management*, 59(2), 77-96.

577 Rosolem, R., H. V. Gupta, W. J. Shuttleworth, X. B. Zeng, and L. G. G. de Goncalves (2012), A
578 fully multiple-criteria implementation of the Sobol' method for parameter sensitivity analysis,
579 *J. Geophys. Res.-Atmos.*, 117. doi:10.1029/2011jd016355.

580 Schaap, M. G., Leij, F. J., & Van Genuchten, M. T. (2001). Rosetta: A computer program for
581 estimating soil hydraulic parameters with hierarchical pedotransfer functions. *Journal of*
582 *Hydrology*, 251(3), 163-176.

583 Schymanski, S. J., M. Sivapalan, M. L. Roderick, J. Beringer, and L. B. Hutley (2008), An
584 optimality-based model of the coupled soil moisture and root dynamics, *Hydrology and Earth*
585 *System Sciences*, 12(3), 913-932.

586 Senay, G. B., Budde, M. E., & Verdin, J. P. (2011). Enhancing the simplified surface energy
587 balance (SSEB) approach for estimating landscape ET: Validation with the METRIC model.
588 *Agricultural Water Management*, 98(4), 606-618.

589 Šimunek, J., Šejna, M., Saito, H., Sakai, M., van Genuchten, M.T. (2013). The HYDRUS-1D
590 Software Package for Simulating the One-Dimensional Movement of Water, Heat, and Multiple
591 Solutes in Variably-Saturated Media, Version 4.17. Department of Environmental Sciences,
592 University of California Riverside, Riverside, California, USA, 307 pp.

593 Soil Survey Staff, Natural Resources Conservation Service, United States Department of Agriculture.
594 Web Soil Survey. Available online at <http://websoilsurvey.nrcs.usda.gov/>. Accessed in July,
595 2016.

- 596 Stoy, P. (2012). Evapotranspiration and energy flux observations from a global tower network with
597 a critical analysis of uncertainties. AGU Fall Meeting Abstracts, 1. pp. 06.
- 598 Suyker, A., Verma, S., Burba, G., Arkebauer, T., Walters, D., & Hubbard, K. (2004). Growing
599 season carbon dioxide exchange in irrigated and rainfed maize. *Agricultural and Forest*
600 *Meteorology*, 124(1), 1-13.
- 601 Suyker, A. E., & Verma, S. B. (2008). Interannual water vapor and energy exchange in an irrigated
602 maize-based agroecosystem. *Agricultural and Forest Meteorology*, 148(3), 417-427.
- 603 Suyker, A. E., & Verma, S. B. (2009). Evapotranspiration of irrigated and rainfed maize–soybean
604 cropping systems. *Agricultural and Forest Meteorology*, 149(3), 443-452.
- 605 Suyker, A. E., Verma, S. B., Burba, G. G., & Arkebauer, T. J. (2005). Gross primary production
606 and ecosystem respiration of irrigated maize and irrigated soybean during a growing season.
607 *Agricultural and Forest Meteorology*, 131(3), 180-190.
- 608 Suyker, A. E., Verma, S. B., Burba, G. G., & Arkebauer, T. J. (2005). Gross primary production
609 and ecosystem respiration of irrigated maize and irrigated soybean during a growing season.
610 *Agricultural and Forest Meteorology*, 131(3), 180-190.
- 611 Turkeltaub, T., Kurtzman, D., Bel, G., & Dahan, O. (2015). Examination of groundwater recharge
612 with a calibrated/validated flow model of the deep vadose zone. *Journal of Hydrology*, 522,
613 618-627.
- 614 Twarakavi, N. K. C., Šimůnek, J., & Seo, S. (2008). Evaluating interactions between groundwater
615 and vadose zone using the HYDRUS-based flow package for MODFLOW. *Vadose Zone*
616 *Journal*, 7(2), 757-768.
- 617 van Genuchten, M. T. (1980). A closed-form equation for predicting the hydraulic conductivity of
618 unsaturated soils. *Soil Science Society of America Journal*, 44(5), 892-898.

- 619 Verma, S. B., Dobermann, A., Cassman, K. G., Walters, D. T., Knops, J. M., Arkebauer, T. J., et
620 al. (2005). Annual carbon dioxide exchange in irrigated and rainfed maize-based
621 agroecosystems. *Agricultural and Forest Meteorology*, 131(1), 77-96.
- 622 Wang, T., & Franz, T. E. (2015). Field observations of regional controls of soil hydraulic
623 properties on soil moisture spatial variability in different climate zones. *Vadose Zone Journal*,
624 14(8)
- 625 Wang, T., Franz, T. E., Yue, W., Szilagyi, J., Zlotnik, V. A., You, J., et al. (2016). Feasibility
626 analysis of using inverse modeling for estimating natural groundwater recharge from a large-
627 scale soil moisture monitoring network. *Journal of Hydrology*, 533, 250-265.
- 628 Wang, T., Franz, T. E., & Zlotnik, V. A. (2015). Controls of soil hydraulic characteristics on
629 modeling groundwater recharge under different climatic conditions. *Journal of Hydrology*,
630 521, 470-481.
- 631 Wang, T., Istanbuluoglu, E., Lenters, J., & Scott, D. (2009a). On the role of groundwater and soil
632 texture in the regional water balance: An investigation of the Nebraska sand hills, USA. *Water*
633 *Resources Research*, 45(10)
- 634 Wang, T., Zlotnik, V. A., Šimunek, J., & Schaap, M. G. (2009b). Using pedotransfer functions in
635 vadose zone models for estimating groundwater recharge in semiarid regions. *Water*
636 *Resources Research*, 45(4)
- 637 Wolf, A., Saliendra, N., Akshalov, K., Johnson, D. A., & Laca, E. (2008). Effects of different eddy
638 covariance correction schemes on energy balance closure and comparisons with the modified
639 bowen ratio system. *Agricultural and Forest Meteorology*, 148(6), 942-952.
- 640 Wood, E. F., Roundy, J. K., Troy, T. J., Van Beek, L., Bierkens, M. F., Blyth, E., et al. (2011).
641 Hyperresolution global land surface modeling: Meeting a grand challenge for monitoring
642 earth's terrestrial water. *Water Resources Research*, 47(5)

- 643 Wösten, J., Pachepsky, Y. A., & Rawls, W. (2001). Pedotransfer functions: Bridging the gap
644 between available basic soil data and missing soil hydraulic characteristics. *Journal of*
645 *Hydrology*, 251(3), 123-150.
- 646 Xia, Y., Ek, M. B., Wu, Y., Ford, T., & Quiring, S. M. (2015). Comparison of NLDAS-2
647 simulated and NASMD observed daily soil moisture. part I: Comparison and analysis. *Journal*
648 *of Hydrometeorology*, 16(5), 1962-1980.
- 649 Xie, Y., Sha, Z., & Yu, M. (2008). Remote sensing imagery in vegetation mapping: A review.
650 *Journal of Plant Ecology*, 1(1), 9-23.
- 651 Yang, H., Dobermann, A., Cassman, K. G., & Walters, D. T. (2004). Hybrid-maize. A Simulation
652 Model for Corn Growth and Yield. Nebraska Cooperative Extension CD, 9.
- 653 Yang, W., Yang, L., & Merchant, J. (1997). An assessment of AVHRR/NDVI-ecoclimatological
654 relations in Nebraska, USA. *International Journal of Remote Sensing*, 18(10), 2161-2180.
- 655 Zhang, L., Dawes, W., & Walker, G. (2001). Response of mean annual evapotranspiration to
656 vegetation changes at catchment scale. *Water Resources Research*, 37(3), 701-708.
- 657 Zhang, Z., Tian, F., Hu, H., & Yang, P. (2014). A comparison of methods for determining field
658 evapotranspiration: Photosynthesis system, sap flow, and eddy covariance. *Hydrology and*
659 *Earth System Sciences*, 18(3), 1053-1072.
- 660 Zreda, M., Shuttleworth, W., Zeng, X., Zweck, C., Desilets, D., Franz, T., et al. (2012). COSMOS:
661 The cosmic-ray soil moisture observing system. *Hydrology and Earth System Sciences*,
662 16(11), 4079-4099.
- 663 Zreda, M., Desilets, D., Ferré, T., & Scott, R. L. (2008). Measuring soil moisture content non-
664 invasively at intermediate spatial scale using cosmic-ray neutrons. *Geophysical Research*
665 *Letters*, 35(21).

666

667 **List of Figures**

668 Figure 1. Study site (Mead Rainfed/US-Ne3) location in Nebraska (a) and locations of Eddy-
669 Covariance Tower (EC), Cosmic-Ray Neutron Probe (CRNP), Theta Probes (TPs), and
670 variability of soil texture based on Web Soil Survey data at the study site, 2014 (b). See table 1
671 for soil descriptions.

672 Figure 2. Eddy-Covariance Tower (a) and Cosmic-Ray Neutron Probe (b) Located at the Mead
673 Rainfed (US-Ne3) Site.

674 Figure 3. Daily precipitation (P) and reference evapotranspiration (ET_r) during the calibration
675 (2008–2010) and validation (2011–2012) periods at the Mead Rainfed (US-Ne3) Site.

676 Figure 4. Temporal evolution of daily SWC (θ) at different soil depths. The black lines represent
677 daily mean SWC (θ) calculated from TPs in 4 different locations at study site and the blue areas
678 indicate one standard deviation.

679 Figure 5. Time series of daily CRNP and spatial average TP SWC (θ) data.

680 Figure 6. Annual precipitation (P) and annual actual evapotranspiration (ET_a) at the Mead Rainfed
681 (US-Ne3) Site.

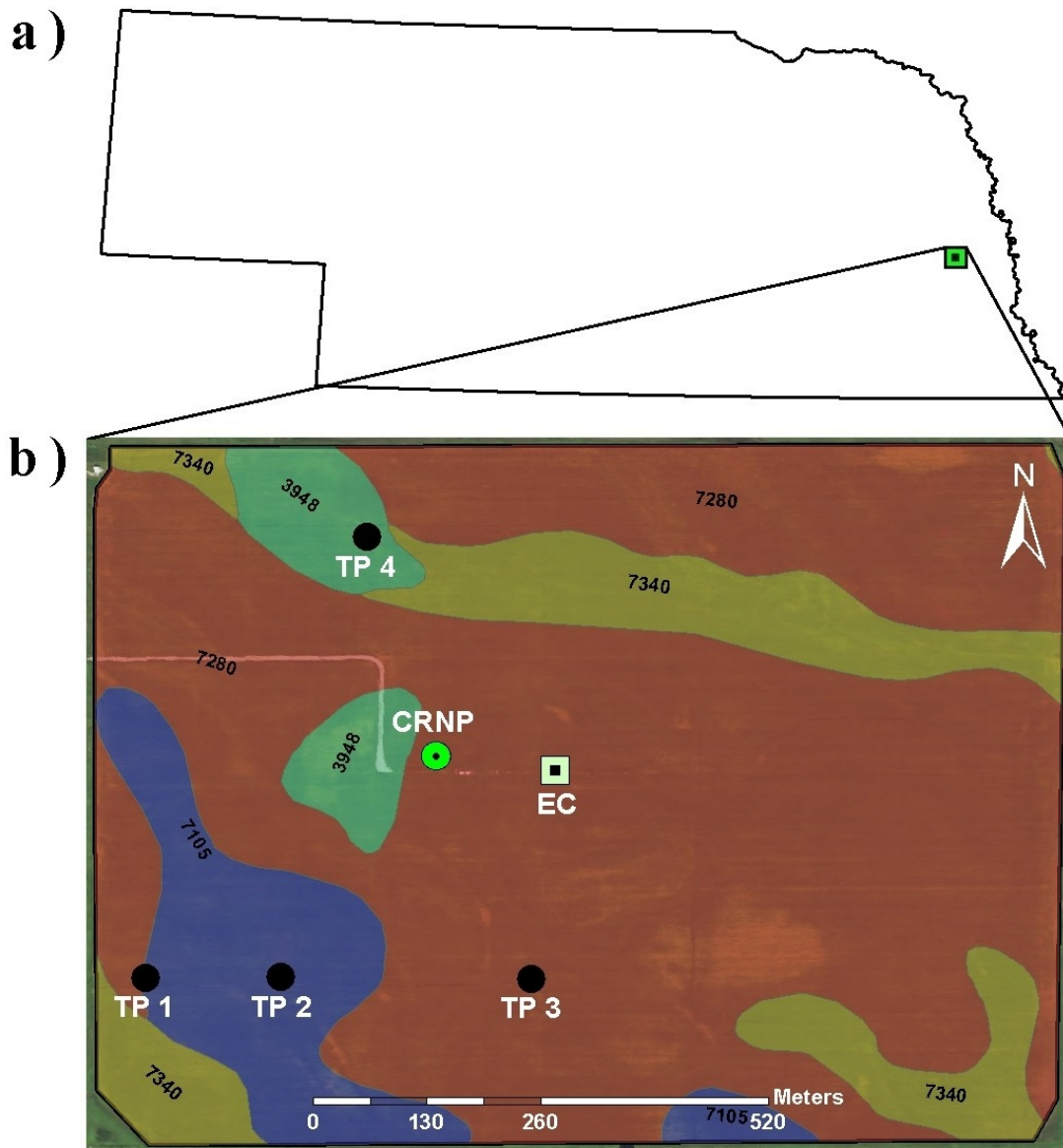
682 Figure 7. Daily observed and simulated SWC (θ) during the calibration (2008–2010) and validation
683 (2011–2012) periods at TP 1 location. See supplemental figures for other comparisons.

684 Figure 8. Daily observed and simulated SWC (θ) during the calibration (2012–2013) and validation
685 (2014) periods at the location of Cosmic-Ray Neutron probe.

686 Figure 9. Simulated daily ET_a versus Observed daily ET_a in different locations at the study site
687 (2007-2012).

688 Figure 10. Sensitivity Analysis of Effect of Soil Hydraulic Parameters on average annual ET_a values
689 (2007-2012) for a single homogeneous soil layer (6 parameters) and for a 4-layer soil profile (24
690 parameters).

691 Figure 11. Sensitivity Analysis of Effect of Root Depth on *ETa* estimation for a single homogeneous
692 soil layer profile. Note that root depth is in terms of percent depth as it is dynamic over the
693 growing period.

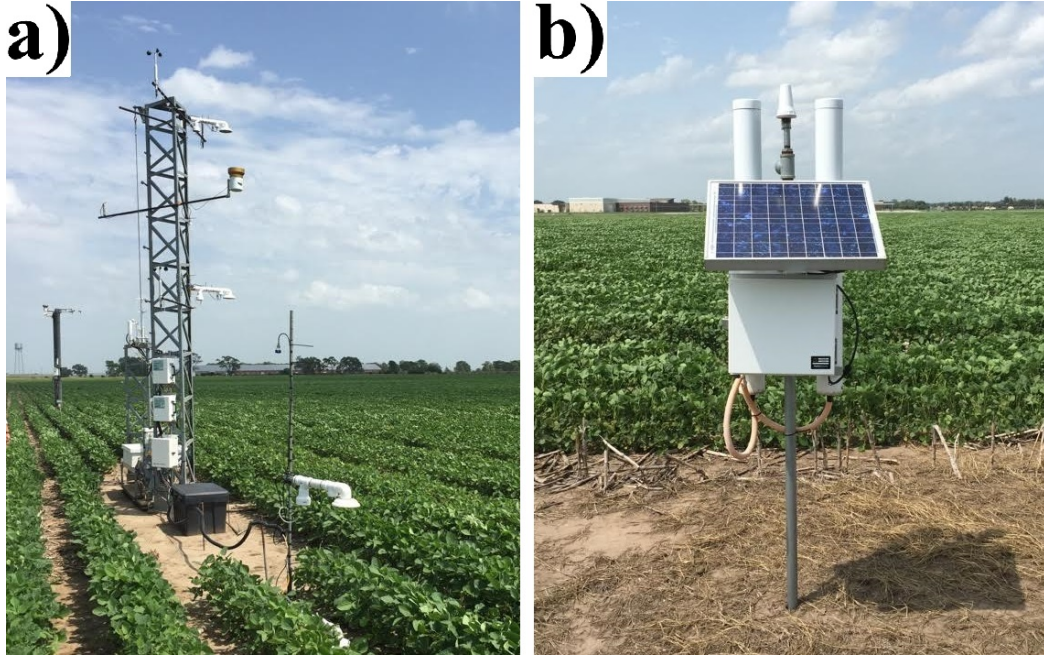


694

695 Figure 1. Study site (Mead Rainfed/US-Ne3) location in Nebraska (a) and locations of Eddy-
 696 Covariance Tower (EC), Cosmic-Ray Neutron Probe (CRNP), Theta Probes (TPs), and
 697 variability of soil texture based on Web Soil Survey data at the study site, 2014 (b). See table 1
 698 for soil descriptions.

699

700

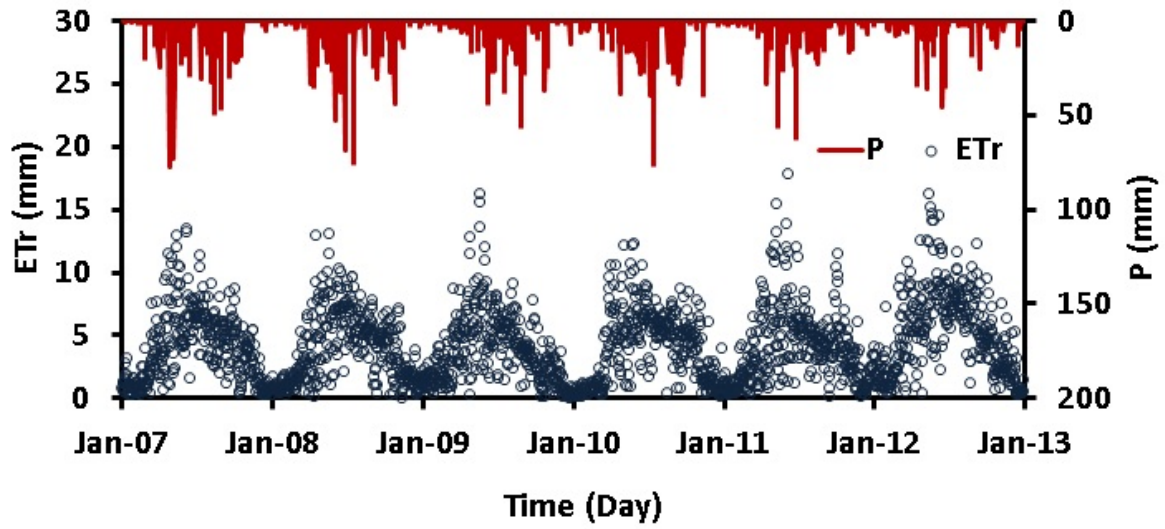


701

702

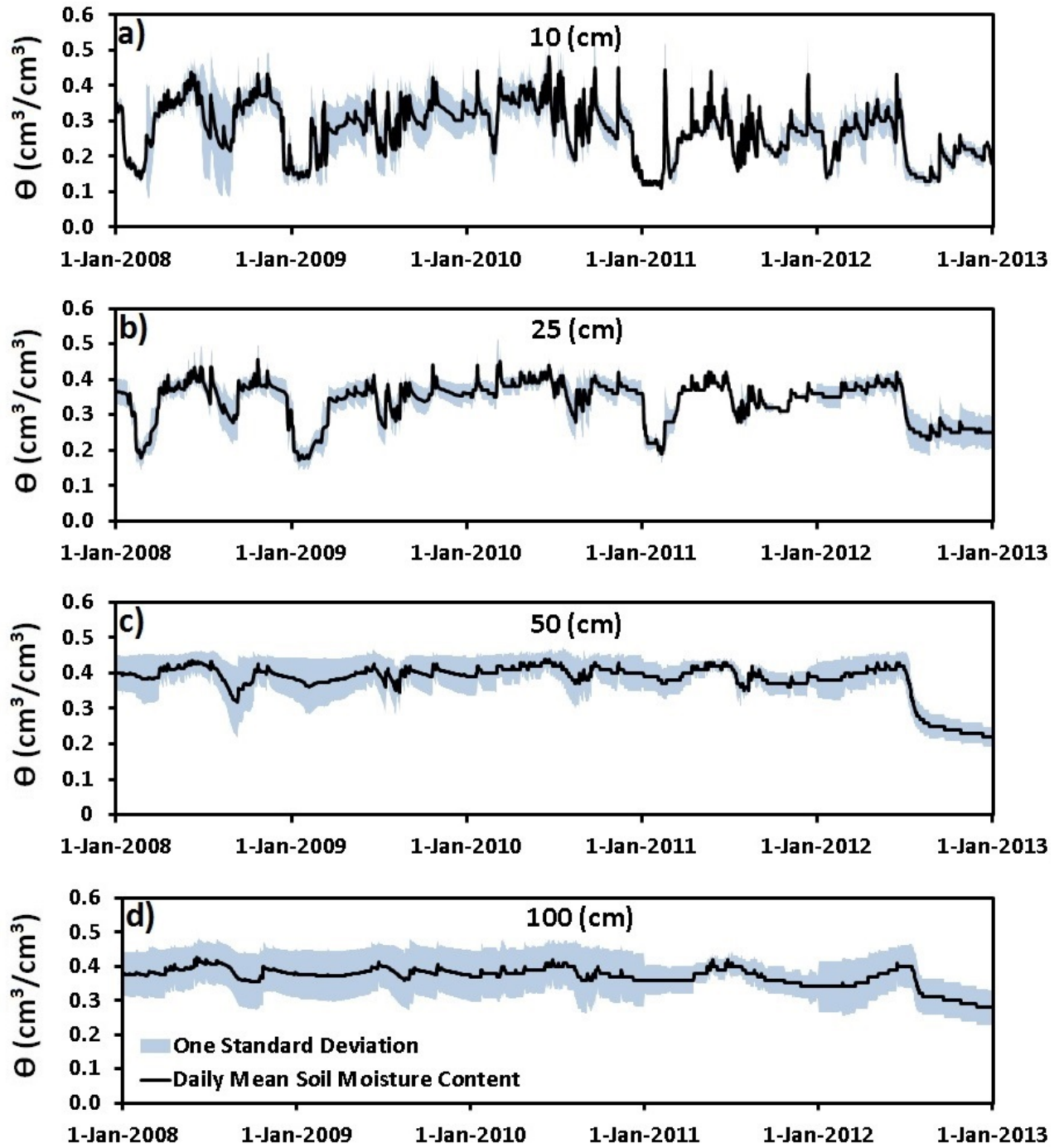
703

Figure 2. Eddy-Covariance Tower (a) and Cosmic-Ray Neutron Probe (b) Located at the Mead Rainfed (US-Ne3) Site.



704
705
706

Figure 3. Daily precipitation (P) and reference evapotranspiration (ET_r) during the calibration (2008–2010) and validation (2011–2012) periods at the Mead Rainfed (US-Ne3) Site.



707

708 Figure 4. Temporal evolution of daily *SWC* (θ) at different soil depths. The black lines represent
 709 daily mean *SWC* (θ) calculated from TPs in 4 different locations at study site and the blue areas
 710 indicate one standard deviation.

711

712

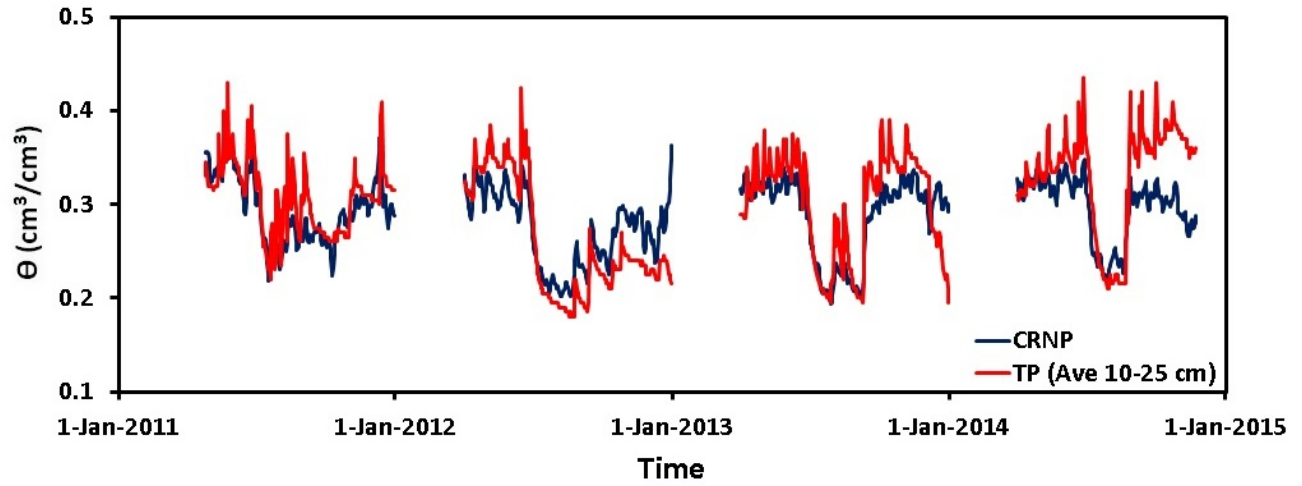
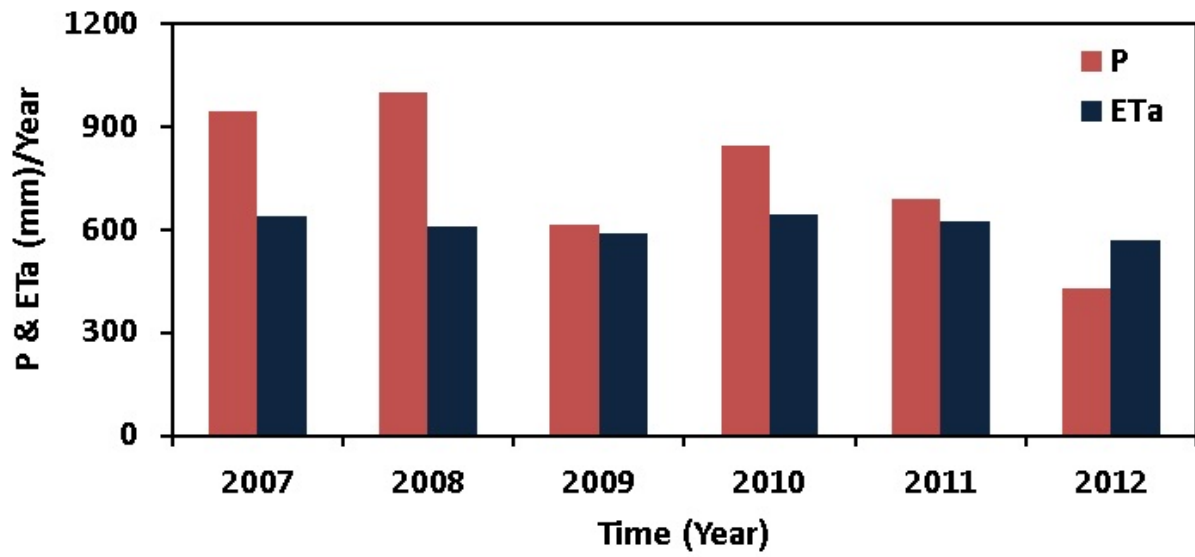


Figure 5. Time series of daily CRNP and spatial average TP *SWC* (θ) data.

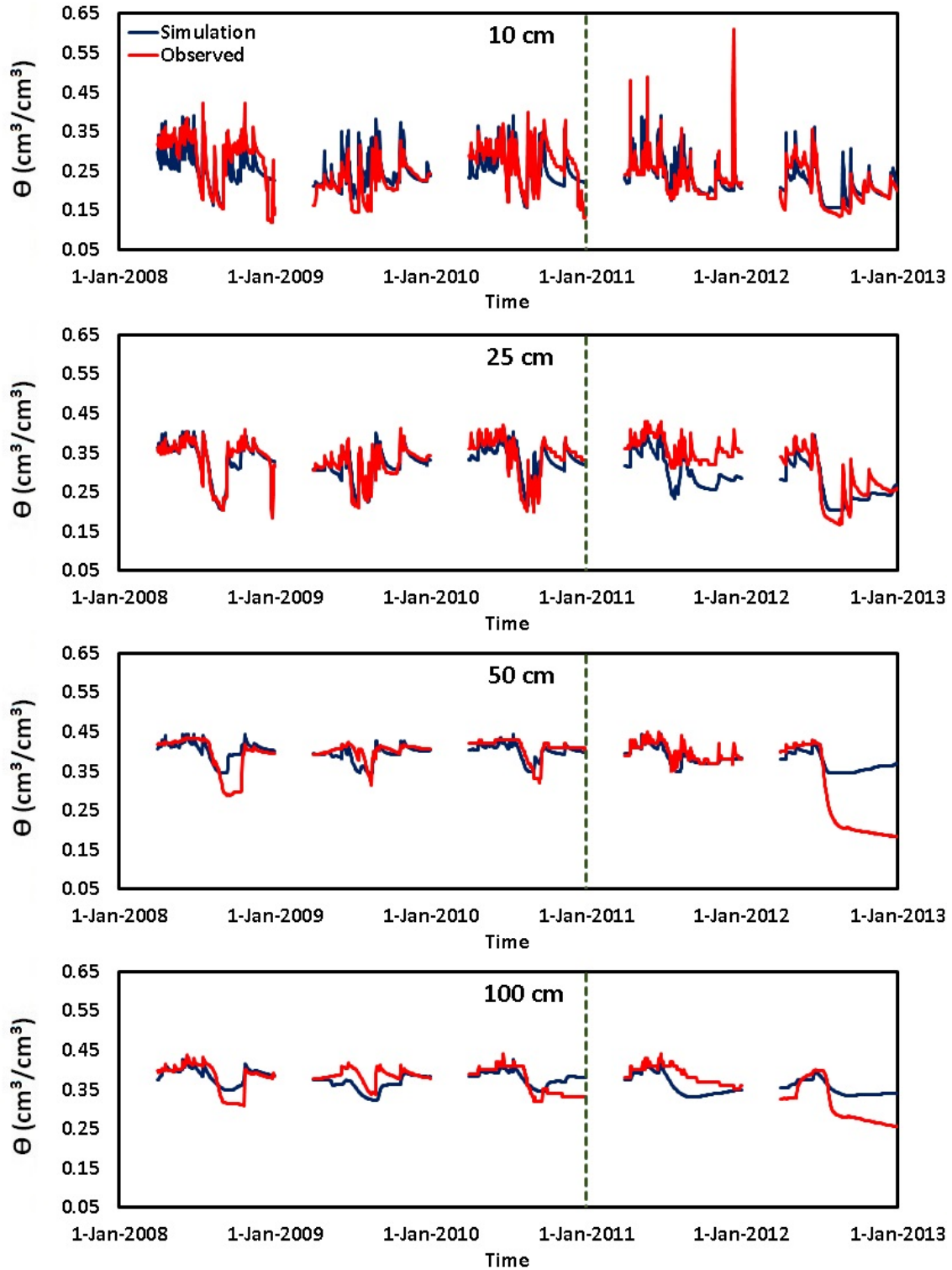
713
 714
 715
 716
 717
 718
 719
 720
 721
 722
 723
 724
 725
 726
 727



728

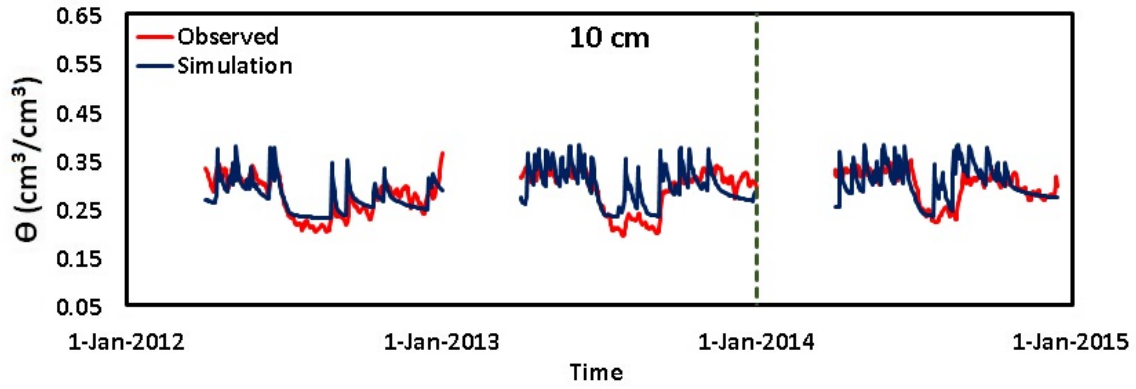
729 Figure 6. Annual precipitation (P) and annual actual evapotranspiration (ET_a) at the Mead Rainfed
 730 (US-Ne3) Site.

731



732

733 Figure 7. Daily observed and simulated *SWC* (θ) during the calibration (2008–2010) and validation
 734 (2011–2012) periods at TP 1 location. See supplemental figures for other comparisons.



735
 736 Figure 8. Daily observed and simulated SWC (θ) during the calibration (2012–2013) and validation
 737 (2014) periods at the location of Cosmic-Ray Neutron probe.

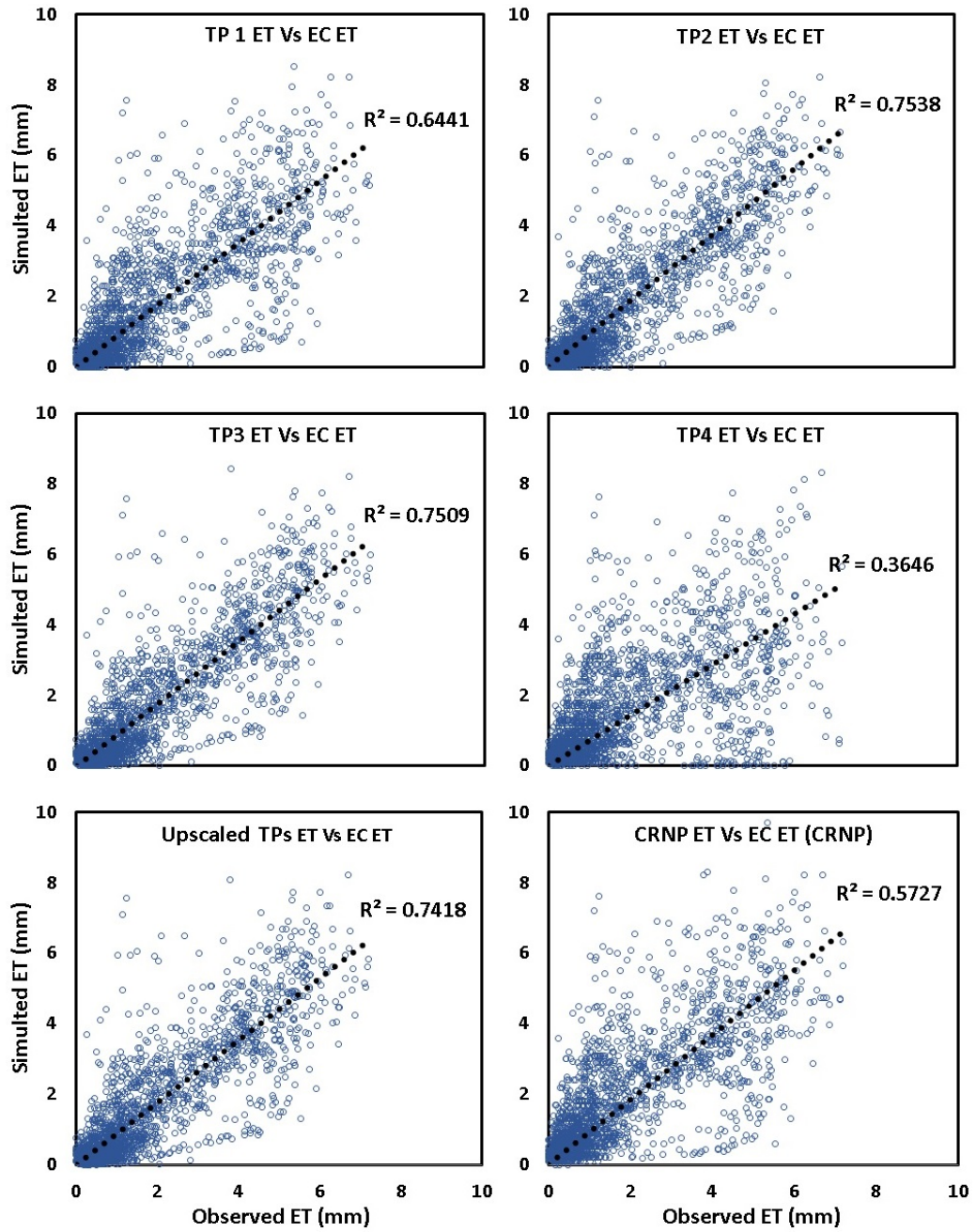
738

739

740

741

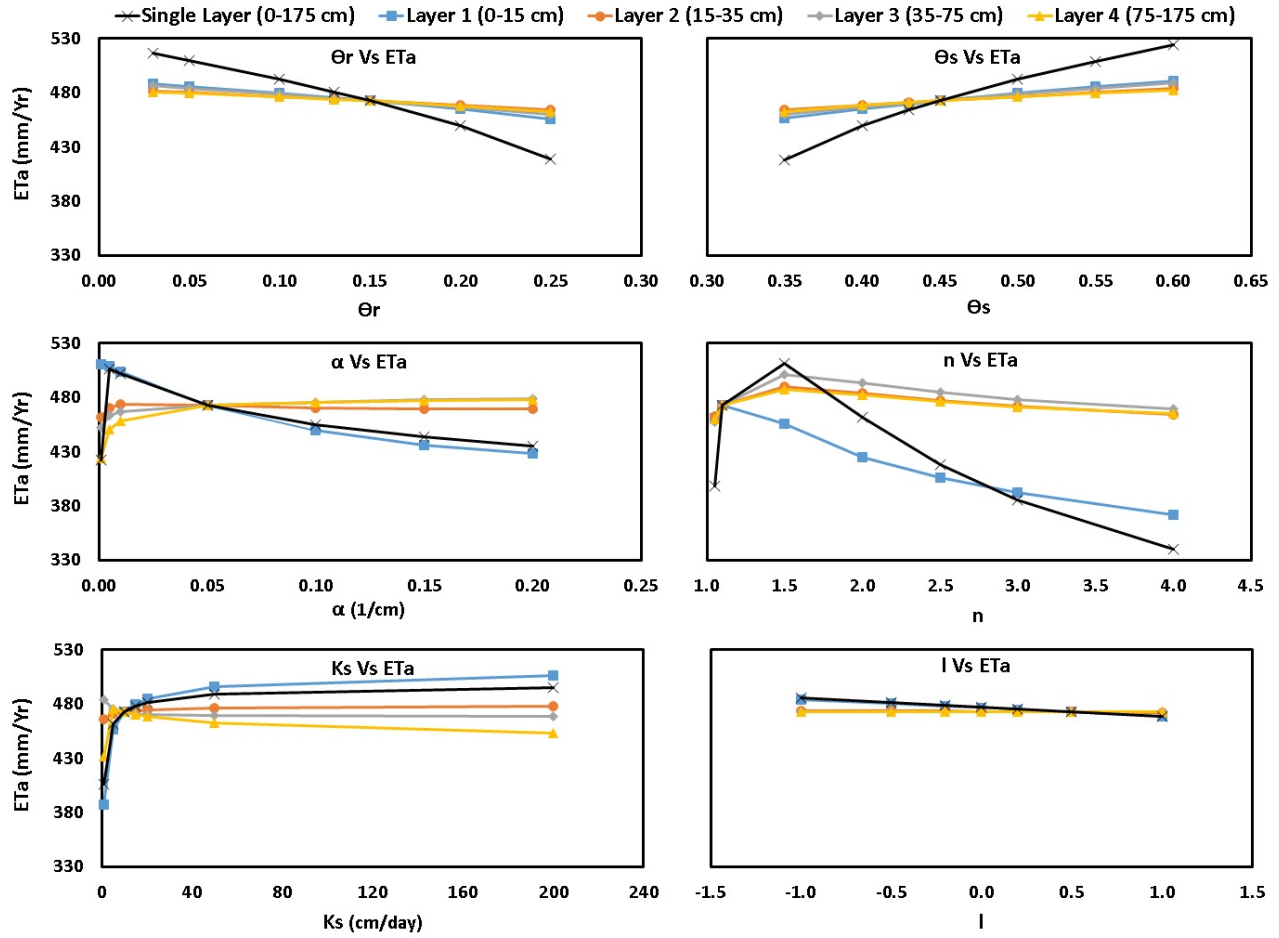
742



743

744 Figure 9. Simulated daily ET_a versus observed daily ET_a at different locations in the study site
 745 (2007-2012).

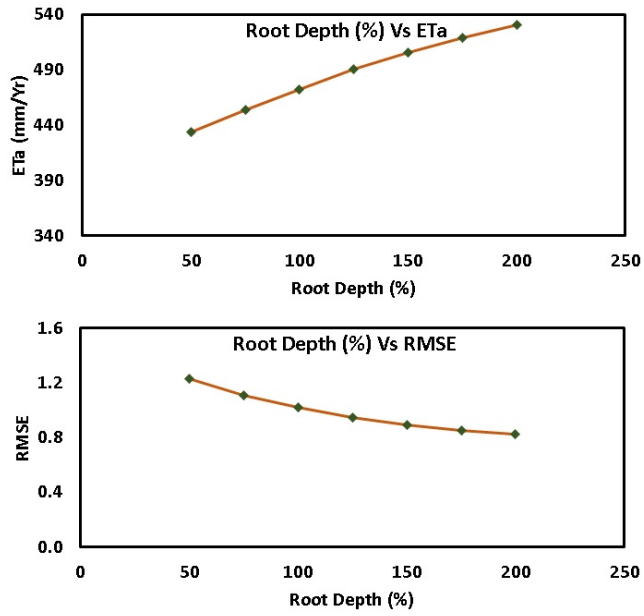
746



747

748 Figure 10. Sensitivity analysis of the effect of soil hydraulic parameters on average annual ET_a
 749 values (2007-2012) for a single homogeneous soil layer (6 parameters) and for a 4-layer soil
 750 profile (24 parameters).

751



752
 753 Figure 11. Sensitivity analysis of root depth on *ETa* estimation for a single homogeneous soil layer
 754 profile. Note that root depth is in terms of percent depth as it is dynamic over the growing period.
 755

756
757
758
759
760
761
762
763
764
765
766
767
768
769
770
771
772
773
774
775
776
777

List of Tables

- Table 1. Variability of soil texture in the study field based on Web Soil Survey data (<http://websoilsurvey.sc.egov.usda.gov/App/HomePage.htm>).
- Table 2. Bounds of the van Genuchten parameters used for inverse modeling.
- Table 3. Goodness-of-fit measures for simulated and observed *SWC* data at different depths during the calibration period (2008 to 2010) and validation period (2011-2012) at TPs locations.
- Table 4. Goodness-of-fit measures for simulated and observed *SWC* data during the calibration period (2012 to 2013) and validation period (2014) at CRNP location.
- Table 5. Optimized van Genuchten parameters in different locations at the study site. Note, 95% confidence intervals are in parentheses.
- Table 6. Goodness-of-fit measures for simulated and observed daily ET_a during the simulation period (2007-2012) at study site.
- Table 7. Summary of simulated yearly and average actual evapotranspiration (ET_a) (mm) and observed yearly and average actual evapotranspiration (ET_a) (mm) from Eddy-Covariance tower during 2007 to 2012.

778

779
780

Table 1. Variability of soil texture in the study field based on Web Soil Survey data (<http://websoilsurvey.sc.egov.usda.gov/App/HomePage.htm>).

Map Unit Symbol	Map Unit Name	Clay (%)	Silt (%)	Sand (%)	Hectares in Field	Percent of Field
3948	Fillmore silt loam, terrace, occasionally ponded	41.7	51.0	7.3	3.24	4.9%
7105	Yutan silty clay loam, terrace, 2 to 6 percent slopes, eroded	25.8	59.4	14.8	6.88	10.3%
7280	Tomek silt loam, 0 to 2 percent slopes	32.3	61.6	6.1	47.23	70.8%
7340	Filbert silt loam, 0 to 1 percent slopes	41.4	51.7	6.9	9.34	14.0%
Total Area of Field					66.69	100.0%

781

782

783

784

785

786

787

788

789

790

791

Table 2. Bounds of the van Genuchten parameters used for inverse modeling.

Soil Parameter	θ_r (-)	θ_s (-)	α (1/cm)	n (-)	K_s (cm/day)	l (-)
Range	0.03–0.30	0.3–0.6	0.001–0.200	1.01–6.00	1–200	-1–1

792

793

794

795

796

797

798

799

800

801

802

803

804

805

806

807 Table 3. Goodness-of-fit measures for simulated and observed *SWC* data at different depths during
 808 the calibration period (2008 to 2010) and validation period (2011-2012) at TPs locations. Note
 809 we assume a good fit as an RMSE between 0-0.03 cm³/cm³ and fair as between 0.03-0.06
 810 cm³/cm³.

Location	Depth (cm)	Calibration Period (2008-2010)				Validation Period (2011-2012)			
		R ²	MAE (cm ³ /cm ³)	RMSE (cm ³ /cm ³)	NSE	R ²	MAE (cm ³ /cm ³)	RMSE (cm ³ /cm ³)	NSE
TP 1	10	0.542	0.024	0.036	0.533	0.532	0.016	0.033	0.503
	25	0.742	0.014	0.022	0.739	0.716	0.029	0.040	0.486
	50	0.409	0.013	0.023	0.407	0.603	0.041	0.074	0.157
	100	0.352	0.015	0.022	0.343	0.419	0.027	0.038	0.358
TP 2	10	0.330	0.044	0.066	0.305	0.287	0.047	0.061	0.052
	25	0.623	0.010	0.020	0.604	0.718	0.038	0.055	0.135
	50	0.551	0.015	0.026	0.074	0.683	0.040	0.055	0.202
	100	0.424	0.019	0.027	-2.055	0.344	0.048	0.073	-0.473
TP 3	10	0.269	0.034	0.051	0.256	0.534	0.086	0.102	-4.265
	25	0.512	0.011	0.017	0.509	0.852	0.010	0.015	0.793
	50	0.549	0.015	0.023	-0.214	0.658	0.022	0.033	0.652
	100	0.238	0.018	0.029	-3.156	0.669	0.018	0.025	0.178
TP 4	10	0.412	0.029	0.044	0.406	0.580	0.051	0.071	-0.116
	25	0.434	0.016	0.025	0.350	0.594	0.029	0.042	0.490
	50	0.151	0.009	0.015	-13.400	0.443	0.041	0.073	0.036
	100	0.001	0.013	0.021	-12.058	0.292	0.026	0.039	0.238

811

812

813

814

815

816

817 Table 4. Goodness-of-fit measures for simulated and observed *SWC* data during the calibration
818 period (2012 to 2013) and validation period (2014) at CRNP location.

Location	Depth (cm)	Calibration Period (2012-2013)				Validation Period (2014)			
		R ²	MAE (cm ³ /cm ³)	RMSE (cm ³ /cm ³)	NSE	R ²	MAE (cm ³ /cm ³)	RMSE (cm ³ /cm ³)	NSE
CRNP	10	0.497	0.018	0.027	0.456	0.192	0.020	0.032	-0.310

819

820

821

822

823

824

825

826

827

828

829

830

831 Table 5. Optimized van Genuchten parameters in different locations at the study site. Note, 95%
 832 confidence intervals are in parentheses.

Location	Depth (cm)	θ_r (-)	θ_s (-)	α (1/cm)	n (-)	K_s (cm/day)	l (-)
TP 1	0-15	0.134 (0.130-0.137)	0.423 (0.417-0.429)	0.027 (0.026-0.027)	1.475 (1.456-1.494)	8.119 (7.965-8.273)	0.546 (0.525-0.567)
	15-35	0.136 (0.132-0.141)	0.408 (0.404-0.412)	0.007 (0.007-0.007)	1.345 (1.322-1.367)	11.540 (11.137-11.939)	0.480 (0.466-0.494)
	35-75	0.191 (0.188-0.194)	0.448 (0.443-0.453)	0.024 (0.024-0.025)	1.097 (1.088-1.105)	8.057 (7.879-8.235)	0.285 (0.278-0.292)
	75-175	0.071 (0.068-0.073)	0.430 (0.424-0.436)	0.025 (0.024-0.025)	1.069 (1.061-1.077)	9.807 (9.540-10.073)	0.364 (0.354-0.375)
TP 2	0-15	0.211 (0.195-0.227)	0.446 (0.431-0.461)	0.027 (0.018-0.035)	1.567 (1.431-1.703)	8.120 (4.660-11.580)	1.000 (0.411-1.589)
	15-35	0.197 (0.105-0.289)	0.434 (0.425-0.442)	0.006 (0.003-0.008)	1.191 (1.076-1.306)	8.655 (0.953-16.357)	0.022 (-0.194-0.238)
	35-75	0.110 (0-0.258)	0.424 (0.406-0.441)	0.015 (0.007-0.023)	1.239 (1.040-1.438)	4.605 (0-9.214)	0.723 (-1.210-2.655)
	75-175	0.109 (0-0.275)	0.408 (0.357-0.459)	0.020 (0-0.044)	1.302 (0.965-1.639)	6.780 (0-20.523)	0.000 (-0.045-0.045)
TP 3	0-15	0.281 (0.276-0.287)	0.464 (0.463-0.465)	0.035 (0.033-0.036)	1.487 (1.446-1.528)	7.096 (6.742-7.450)	0.400 (0.385-0.416)
	15-35	0.072 (0.069-0.075)	0.402 (0.398-0.407)	0.012 (0.011-0.012)	1.085 (1.076-1.095)	29.960 (28.470-31.457)	0.353 (0.340-0.367)
	35-75	0.081 (0.076-0.087)	0.498 (0.481-0.515)	0.037 (0.034-0.039)	1.128 (1.108-1.149)	24.440 (22.013-26.872)	0.527 (0.472-0.583)
	75-175	0.085 (0.077-0.092)	0.500 (0.482-0.518)	0.039 (0.036-0.042)	1.147 (1.124-1.170)	17.540 (15.995-19.088)	0.496 (0.454-0.539)
TP 4	0-15	0.082 (0.069-0.096)	0.481 (0.474-0.489)	0.034 (0.030-0.038)	1.172 (1.158-1.186)	7.773 (6.913-8.632)	0.953 (0.772-1.133)
	15-35	0.200 (0.175-0.225)	0.426 (0.420-0.433)	0.013 (0.010-0.017)	1.217 (1.173-1.262)	14.060 (9.248-18.873)	0.044 (0.027-0.061)
	35-75	0.250 (0.240-0.260)	0.477 (0.472-0.481)	0.009 (0.007-0.011)	1.079 (1.066-1.092)	1.045 (0.952-1.138)	0.353 (0.168-0.538)
	75-175	0.200 (0.185-0.214)	0.487 (0.481-0.494)	0.012 (0.009-0.014)	1.070 (1.057-1.083)	1.454 (1.146-1.762)	0.985 (0.706-1.264)
CRNP	0-15	0.100 (0.098-0.103)	0.392 (0.386-0.398)	0.019 (0.018-0.019)	1.054 (1.145-1.164)	6.931 (6.786-7.076)	0.547 (0.545-0.549)

833

834
835

Table 6. Goodness-of-fit measures for simulated and observed daily ET_a during the simulation period (2007-2012) at study site.

Location	R ²	MAE (mm/day)	RMSE (mm/day)	NSE
TP 1	0.644	0.696	1.062	0.618
TP 2	0.754	0.610	0.907	0.746
TP 3	0.751	0.601	0.904	0.728
TP 4	0.365	0.878	1.387	0.168
TPs Weighted Average	0.742	0.599	0.911	0.714
CRNP	0.573	0.742	1.143	0.562

836

837

838

839

840

841

842

843

844

845

846

847

848

849 Table 7. Summary of simulated yearly and average actual evapotranspiration (ET_a) (mm) and
 850 observed yearly and average actual evapotranspiration (ET_a) (mm) from Eddy-Covariance
 851 tower during 2007 to 2012.

Location	Year						
	2007	2008	2009	2010	2011	2012	Average
EC	656.8	608.4	589.7	646.1	622.2	570.1	612.5
TP 1	646.1	629.0	559.8	642.1	573.9	415.5	579.5
TP 2	614.3	598.4	576.7	620.5	576.9	429.5	574.7
TP 3	529.0	556.1	556.4	590.4	549.8	405.2	545.4
TP 4	652.2	576.1	529.9	677.3	458.2	381.2	525.3
Upscaled TPs	613.9	564.1	556.3	600.3	547.7	405.9	548.0
CRNP	745.3	707.1	603.0	721.8	642.2	439.3	643.1

852